PKA regulation of neuronal function requires the dissociation of catalytic subunits from regulatory subunits

Wei-Hong Xiong, Maozhen Qin, and Haining Zhong

Vollum Institute, Oregon Health & Science University, Portland, OR 97239, USA

Correspondence should be addressed to H.Z. (email: zhong@ohsu.edu).

Haining Zhong, Ph.D.
Vollum Institute, Oregon Health & Science University
3181 SW Sam Jackson Park Road, L474
Portland, Oregon 97239
U.S.A.
(503) 494-5089 / zhong@ohsu.edu

Key words: cAMP-dependent kinase / protein kinase A (PKA); two-photon imaging; norepinephrine; shRNA knockdown; late-phase structural long-term potentiation; AMPA and NMDA-mediated synaptic transmission.

Abstract

Protein kinase A (PKA) plays essential roles in diverse cellular functions. However, the spatiotemporal dynamics of endogenous PKA upon activation remain debated. The classical model predicts that PKA catalytic subunits dissociate from regulatory subunits in the presence of cAMP, whereas a second model proposes that catalytic subunits remain associated with regulatory subunits following physiological activation. Here we report that different PKA subtypes, as defined by the regulatory subunit, exhibit distinct subcellular localization at rest in CA1 neurons of cultured hippocampal slices. Nevertheless, when all tested PKA subtypes are activated by norepinephrine, presumably via the β-adrenergic receptor, catalytic subunits translocate to dendritic spines but regulatory subunits remain unmoved. These differential spatial dynamics between the subunits indicate that at least a significant fraction of PKA dissociates. Furthermore, PKA-dependent regulation of synaptic plasticity and transmission can be supported only by wildtype, dissociable PKA, but not by inseparable PKA. These results indicate that endogenous PKA regulatory and catalytic subunits dissociate to achieve PKA function in neurons.

31 **Introduction**

32 Cyclic adenosine monophosphate (cAMP)-dependent kinase, or protein kinase A (PKA),
33 regulates diverse critical functions in nearly all mammalian cells, including neurons. PKA is
34 a tetrameric protein consisting of two regulatory subunits (PKA-Rs) and two catalytic
35 subunits (PKA-Cs) (Francis and Corbin, 1994; Johnson et al., 2001). In the inactive state,
36 each PKA-R binds to and inhibits a PKA-C. Binding of cAMP to PKA-R activates PKA-C.
37 However, there are different proposals on the molecular events that follow activation.

38 For decades, PKA-C is thought to dissociate from PKA-R upon cAMP binding (Beavo
39 et al., 1974; Francis and Corbin, 1994; Gold, 2019; Johnson et al., 2001; Reimann et al.,
40 1971). Freed PKA-C molecules then move to phosphorylate their substrates. However,
41 several studies (reviewed in Gold, 2019), including two notable recent publications (Smith
42 et al., 2017, 2013), propose an alternative model, in which physiological concentrations of
43 cAMP can activate PKA-C but do not result in its dissociation from PKA-R. Testing these two
44 models will not only elucidate the biophysical mechanism of PKA activation, but also have
45 distinct implications in how PKA may achieve its specificity, which is thought to rely on
46 spatial compartmentalization (Wong and Scott, 2004).

47 We have previously found that the majority of type IIβ PKA, as defined by PKA-R, is
48 anchored to microtubules in the dendritic shaft of hippocampal CA1 pyramidal neurons
49 where PKA-RIIβ is bound to the abundant microtubule associated protein MAP-2 (Zhong et
50 al., 2009). Upon activation of the β-adrenergic receptor with norepinephrine, a fraction of
51 PKA-C dissociated from PKA-RIIβ (Tillo et al., 2017). The freed PKA-C redistributed into
52 dendritic spines, whereas PKA-RIIβ remained anchored at the dendritic shaft (Tillo et al.,

53 2017; Xiong et al., 2021). These results are consistent with the classical PKA activation
54 model. However, recent studies suggest that PKA-Rs other than PKA-RIIβ may be the more
55 abundant isoforms in CA1 neurons (Church et al., 2021; Ilouz et al., 2017; Weisenhaus et al.,
56 2010). It remains untested whether these PKA isoforms dissociate upon physiologically
57 relevant stimulations in neurons.

58 Here, we examined whether PKA-C dissociates from all major PKA-R isoforms in
59 CA1 neurons. The rescue of function following knockdown of PKA-C was compared
60 between wildtype dissociable PKA and an inseparable PKA variant in which PKA-C is
61 covalently linked to PKA-R. The results support the classical model of PKA activation via
62 dissociation.

63 **Results**

64 Recent studies have suggested that PKA-RIIα and PKA-RIβ may be the prevalent
65 isoforms in hippocampal CA1 neurons. Therefore, we co-expressed C-terminally
66 monomeric EGFP tagged PKA-C (PKA-C-mEGFP) (Tillo et al., 2017; Zhong et al., 2009) and a
67 cytosolic marker (mCherry) with either PKA-RIIα or PKA-RIβ in CA1 neurons of
68 organotypic hippocampal slice cultures (Figs. 1A and 1B, upper left panels). At rest, PKA-C-
69 mEGFP exhibited a distribution that was dependent on the co-expressed PKA-R: when co-
70 expressed with PKA-RIIα, PKA-C was enriched in dendritic shafts; when co-expressed with
71 PKA-RIβ, PKA-C was more evenly distributed (quantified using the spine enrichment
72 indexes, or SEI, see Methods) (Fig. 1C). This distribution was independent of the expression
73 level (rest conditions in Figure 1–figure supplement 1) and largely resembled that of the

74 corresponding PKA-R, as visualized using expressed PKA-R-mEGFP in separate
75 experiments (Figs. 1A-1C).

76 Notably, upon application of norepinephrine (10 μM), PKA-C of both subtypes
77 translocated to dendritic spines, but the subcellular localization of PKA-Rs remained
78 unchanged (Figs. 1D & 1E). A 5x lowered norepinephrine concentration (2 μM) also
79 resulted in similar dynamics of PKA-C (Figure 1–figure supplement 2), indicating that the
80 PKA-C translocation happens in a wide range of neuromodulator concentrations. This
81 differential re-distribution between PKA-C and PKA-R was more prominent following
82 activation with forskolin (25 μM) and IBMX (50 μM). The translocation of PKA-C was
83 independent of the expression level and the effect remained when extrapolating to the
84 zero-overexpression level using a linear fit (Figure 1–figure supplement 1). These results
85 can only be explained if at least a fraction of PKA-C dissociated from both PKA-RIIα and
86 PKA-RIβ when a physiological stimulant was used. The differential re-distribution between
87 PKA-C and PKA-R was also observed when PKA-RIα was used (Figure 1–figure supplement
88 3), although it was less implicated in hippocampal neurons. Together with our earlier
89 results regarding PKA-C/PKA-RIIβ, we conclude that PKA-C dissociates from PKA-R with
90 physiologically relevant stimuli.

91 Next, we asked whether PKA regulation of neuronal function is dependent on the
92 dissociation of PKA-C from PKA-R. A key experiment supporting the non-dissociating PKA
93 activation model was that PKA regulation of cell growth could be sustained by a construct
94 in which PKA-C was fused to PKA-RIIα in one polypeptide chain via a flexible linker (named
95 R-C; Fig. 2A) (Smith et al., 2017). We therefore asked whether this R-C construct could

96 support PKA regulation of neuronal function. When R-C-mEGFP was expressed in CA1
97 neurons, this construct exhibited a distribution highly similar to that of RIIα (Figs. 2B and
98 2C). The tendency of this construct to translocate to the spine was largely diminished
99 compared to PKA-C-mEGFP co-expressed with wildtype, unlinked PKA-RIIα (Fig. 2D),
100 indicating that the catalytic subunit in R-C was indeed inseparable from the regulatory
101 subunit.

102 To evaluate the function of R-C, a previously established shRNA construct was used
103 to selectively knock down PKA-Cα in CA1 neurons in cultured hippocampal slices (Tillo et
104 al., 2017). Given that PKA activation is required for the late phase of long-term potentiation
105 (L-LTP) (Abel et al., 1997), we examined the structural LTP of individual dendritic spines of
106 CA1 neurons elicited by focal two-photon glutamate uncaging (Fig. 3) (Matsuzaki et al.,
107 2004). The shRNA knockdown of PKA-C resulted in attenuated LTP at 90 min after
108 induction (Figs. 3A–3C). This attenuation was not observed when a control shRNA against
109 LacZ was expressed (Fig. 3C). The attenuated structural LTP was rescued by co-expression
110 of shRNA-resistant wild-type PKA-C-mEGFP together with PKA-RIIα (Figs. 3A–3C).
111 However, the R-C construct in which PKA-C was also resistant to shRNA knockdown but
112 could not leave PKA-RIIα failed to rescue the phenotype.

113 PKA activity has also been shown to regulate synaptic transmission. We therefore
114 examined evoked AMPA and NMDA receptor (AMPAR and NMDAR, respectively) currents
115 in paired, transfected and adjacent untransfected CA1 neurons in cultured hippocampal
116 slices. As shown previously (Tillo et al., 2017; Xiong et al., 2021), neurons expressing the
117 shRNA construct against PKA-C exhibited significantly lower AMPAR currents (Fig. 4A), but

118 not NMDAR currents (Fig. 4B). As a result, the AMPAR/NMDAR current ratio was also
119 reduced (Fig. 4C). The deficits were rescued by co-expression of shRNA-resistant, wild-type
120 dissociable PKA-C-mEGFP and PKA-RIIα (Fig. 4). However, the inseparable R-C construct
121 failed to rescue the phenotype. Taken together, the R-C construct did not support normal
122 PKA-dependent synaptic function.

123 **Discussion**

124 Our results indicate that at least a fraction of PKA-C molecules dissociate from all
125 tested PKA-R isoforms, including Iβ, IIα and previously tested IIβ, when activated by
126 physiological stimuli. Given that PKA activity increases by two orders of magnitude when
127 dissociated from PKA-R (Miyamoto et al., 1969), even a small fraction of PKA-C dissociation
128 will result in a marked increase of PKA kinase activity. These results corroborate the
129 observations in intact non-neuronal cells that used FRET imaging and biochemical
130 measurements, respectively (Walker-Gray et al., 2017; Zaccolo et al., 2000). Furthermore,
131 PKA-C that is covalently linked to PKA-RIIα cannot functionally replace wildtype PKA for
132 normal neuronal transmission or plasticity. Although this R-C construct has been shown to
133 functionally replace endogenous PKA in terms of supporting the growth of a heterologous
134 cell line (Smith et al., 2017), it cannot support all necessary PKA functions. Overall, we
135 conclude that PKA-C dissociation from PKA-R is essential for PKA regulation of neuronal
136 function. Additionally, PKA specificity is mediated by spatial compartmentalization (Wong
137 and Scott, 2004). This is likely mediated by mechanism downstream of PKA dissociation,
138 such as membrane tethering of freed PKA-C or its buffering by extra PKA-Rs (Gaffarogullari
139 et al., 2011; Tillo et al., 2017; Walker-Gray et al., 2017; Zhang et al., 2015).

140 In addition, this study shows that PKA distribution in neuronal dendrites at the
141 resting state is subtype dependent. PKA-RIIα is enriched in dendritic shaft in a way similar
142 to PKA-RIIβ, likely via its interaction with the abundant microtubule binding protein MAP2
143 (Tillo et al., 2017; Vallee et al., 1981). Note that this observation does not exclude the
144 importance a small fraction of PKA being anchored to synaptic sites via other PKA binding
145 proteins. In contrast, PKA-RIα and PKA-RIβ are more evenly distributed between spine and
146 dendrites. These observations establish a spatial organizational base for understanding
147 subtype-specific PKA function in neurons.

148 This study also demonstrates that PKA is essential for long-term structural LTP of
149 individual spines. PKA has been shown to facilitate the induction of LTP (i.e.,
150 metaplasticity) (Thomas et al., 1996; Zhong et al., 2009), and is required for the
151 maintenance of L-LTP (Abel et al., 1997), as assayed using electrophysiological recording of
152 postsynaptic currents. However, it has been suggested that the structural and synaptic
153 current changes may not be causally linked (Kopec et al., 2006). Our results fill the gap to
154 show that PKA is also required for maintaining the late phase of structural LTP.

Materials and Methods

Key Resources Table				
Reagent type (species) or resource	**Designation**	**Source or reference**	**Identifiers**	**Additional information**
strain, strain background (Rattus norvegicus, Sprague Dawley)	Sprague Dawley rat	Charles River	Strain Code 001; RRID: RGD_734476	
recombinant DNA reagent	PKA-Cα-mEGFP (plasmid)	Addgene	# 45524	
recombinant DNA reagent	PKA-RIα-mEGFP (plasmid)	Addgene	# 45525	
recombinant DNA reagent	PKA-RIβ-mEGFP (plasmid)	Addgene	# 45526	
recombinant DNA reagent	PKA-RIIα-mEGFP (plasmid)	Addgene	# 45527	
recombinant DNA reagent	PKA-RIα (plasmid)	This paper		

recombinant DNA reagent	PKA-RIβ (plasmid)	This paper		
recombinant DNA reagent	PKA-RIIα (plasmid)	Addgene	#168492	
recombinant DNA reagent	PKA-RIIα-PKA-Cα-mEGFP (plasmid)	This paper		
recombinant DNA reagent	shPKA against PKA-Cα with DsRed co-expression (plasmid)	This paper		The shRNA was developed in Tillo et al, 2017
recombinant DNA reagent	shPKA against LacZ with DsRed co-expression (plasmid)	This paper		
recombinant DNA reagent	mCherry2 (plasmid)	Addgene	#54517	
chemical compound, drug	norepinephrine	Tocris	5169	
chemical compound, drug	forskolin	LC Labs	F-9926	

chemical compound, drug	IBMX	Sigma-Aldrich	I7018	
chemical compound, drug	MNI-glutamate	Tocris	1490	
chemical compound, drug	TTX	Tocris	1069	
chemical compound, drug	2-chloroadenosine	Sigma-Aldrich	C5134	
chemical compound, drug	GABAzine (SR 95531)	Tocris	1262	
software, algorithm	MATLAB	MathWorks	RRID: SCR_001622; https://www.mathworks.com/	
software, algorithm	SI_View	Github / Zhong Lab	https://github.com/HZhongLab/SI_View	

157 **Plasmid constructs**

158 Constructs were made using standard mutagenesis and subcloning methods. All previously
159 unpublished constructs and their sequences will be submitted to Addgene. In the R-C
160 construct, mouse PKA-RIIα and PKA-Cα were fused via a linker with residues
161 WDPGSGSLEAGCKNFFPRSFTSCGSLEGGSAAA that were previously used (Smith et al.,
162 2017).

163 **Organotypic hippocampal slice cultures and transfections**

164 Cultured rat hippocampal slices were prepared from P6 – P8 (typically P7) pups, as
165 described previously (Stoppini et al., 1991; Zhong et al., 2009). Animal experiments were
166 performed in accordance with the Guide for the Care and Use of Laboratory Animals of the
167 National Institutes of Health, and were approved by the Institutional Animal Care and Use
168 Committee (IACUC) of the Oregon Health & Science University (#IP00002274). cDNA
169 constructs were transfected after 1.5–3 weeks *in vitro* via the biolistic gene transfer
170 method using the Helios gene gun and 1.6 µm gold beads (Fig. 1) or, where long-term
171 expression (~ 1 week) was required, with single-cell electroporation (Fig. 2) (Otmakhov
172 and Lisman, 2012).

173 **Two-photon imaging and two-photon glutamate uncaging**

174 A custom built two-photon microscope based on an Olympus BW51WI microscope body
175 was used. Laser beams from two different Ti:Sapphire lasers (Maitai, Newport) were
176 aligned to allow for simultaneous two-photon excitation and photoactivation. Laser
177 intensities were controlled by Pockels cells (Conoptics). Imaging and photoactivation were
178 controlled by ScanImage (Vidrio Tech) (Pologruto et al., 2003). Slices were perfused during

179 imaging in gassed artificial cerebral spinal fluid (ACSF) containing (mM) 127 NaCl, 25
180 $NaHCO_3$, 25 D-glucose, 2.5 KCl, 4 $MgCl_2$, 4 $CaCl_2$, and 1.25 NaH_2PO_4 with 0.5 μM
181 tetrodotoxin (TTX). mEGFP fluorescence (green) was unmixed from that of the cytosolic
182 marker (mCherry or DsRed Express) using a dichroic (Chroma 565DCXR) and band-pass
183 filters (Chroma HQ510/70 for green and Semrock FF01-630/92 for red).

184 For single-spine structural LTP experiments, 2.25 mM MNI-caged-L-glutamate
185 (Tocris) was added to ACSF containing 4 mM calcium, 0.05 mM magnesium, 1 μM TTX and
186 4 μM 2-chloroadenosine, as previously described (Harvey et al., 2008a). To trigger
187 structural plasticity, 30 pulses of 4-ms 16-mW (at back focal plane) 720-nm laser light
188 were delivered to the spine head at 0.5 Hz.

189 Image analysis was performed using custom software written in MATLAB called
190 *SI_View* (https://github.com/HZhongLab/SI_View) (Ma et al., 2022). Using the software,
191 regions of interest (ROIs) were manually drawn to isolate spines or their immediately
192 adjacent dendritic shaft. Only the spines well isolated from the dendrite laterally
193 throughout the entire experiments were included. Spine enrichment index was calculated
194 as:

195 $$SEI = \log_2[(F_{green}/F_{red})_{spine}/(F_{green}/F_{red})_{shaft}]$$

196 in which F is the average fluorescence intensity in an ROI.

197 The expression level was estimated by the maximal intensity from thick apical
198 dendrite near the soma (typically 50-100 μm) similar to previously described (Harvey et
199 al., 2008b; Tillo et al., 2017). To minimize the influence of noise, a line of 9 pixels (pixel size

200 ~0.04 μm) thick was manually drawn transecting the dendrite through the visually
201 identified, brightest region. The line profile was further smoothened by 5 pixels along the
202 line and baseline subtracted before determining the maximal value. To combine
203 measurements from different hardware configuration (e.g., different microscopes), the data
204 from each configuration and experiment were internally corrected for laser stimulation
205 intensity and then normalized to the average of all data under the same condition.

206 **Electrophysiology**

207 Whole-cell voltage-clamp recordings were performed using a MultiClamp 700B amplifier
208 (Molecular Devices). Electrophysiological signals were filtered at 2 kHz and digitized and
209 acquired at 20 kHz using custom software written in MATLAB. Slices were perfused with
210 artificial cerebrospinal fluid containing 4 mM Ca and 4 mM Mg. The internal solution
211 contained (in mM) 132 Cs-gluconate, 10 HEPES, 10 Na-phosphocreatine, 4 MgCl2, 4 Na2-
212 ATP, 0.4 Na-GTP, 3 Na-ascorbate, 3 QX314, and 0.2 EGTA with an osmolarity of 295
213 mOsmol/kg. The junction potential was calculated to be -17 mV using a built-in function in
214 the Clampfit software (Molecular Devices). Several less abundant anions (phosphocreatine,
215 ATP, GTP and ascorbate) were omitted in the calculation due to lack of data in the program.
216 The Cl reversal potential was -75 mV.

217 To reduce recurrent activities, cultured hippocampal slices were cut on both sides of
218 CA1 and 4 μM 2-chloroadenosine (Sigma) was present in all recording experiments. 10 μM
219 GABAzine (SR 95531, Tocris) was also included to suppress GABA currents. For electrical
220 stimulation, a bipolar, θ-glass stimulating electrode (Warner Instruments) was positioned
221 in the stratum radiatum 100–150 μm lateral to the recorded neuron. For all recordings, a

222 transfected neuron and an untransfected neuron located within 50 μm of each other were
223 sequentially recorded without repositioning the stimulation electrode. Measurements were
224 carried out on averaged traces from approximately 20 trials under each condition. For
225 AMPAR currents, the cells were held at -60 mV (before correcting for the junction
226 potential) and the current was measured as the baseline-subtracted peak current within a
227 window of 2–50 ms after electric stimulation. For NMDAR currents, the average currents at
228 140 to 160 ms after stimulation were used when the cells were held at +55 mV (before
229 correcting for the junction potential)

230 **Data analysis, presentation, and statistics**

231 Quantification and statistical tests were performed using custom software written in
232 MATLAB. Averaged data are presented as mean ± s.e.m., unless noted otherwise. p values
233 were obtained from one-way ANOVA tests, unless noted otherwise. In all figures, *: $p \leq 0.05$
234 and is considered statistically significant after Bonferroni correction for multiple tests, **: p
235 ≤ 0.01, and ***: $p \leq 0.001$.

236

Acknowledgements

We thank all members of the Mao and Zhong laboratories at the Vollum Institute for constructive discussions. We thank Drs John Williams and Michael Muniak for critical comments and edits on the manuscript. This work was supported by two NIH BRAIN Initiative awards to H.Z. (U01NS094247 and R01NS127013).

Author contributions

H.Z. conceived the project. W.X. and H.Z. designed the experiments. W.X. and H.Z. performed the experiments and data analyses. M.Q. produced critical reagents used in the experiments. H.Z. wrote the manuscript.

Competing interests

The authors declare no competing interests.

250 **References**

251 Abel T, Nguyen P V., Barad M, Deuel TAS, Kandel ER, Bourtchouladze R. 1997. Genetic
252 demonstration of a role for PKA in the late phase of LTP and in hippocampus-based
253 long-term memory. *Cell* **88**:615–626. doi:10.1016/S0092-8674(00)81904-2

254 Beavo JA, Bechtel PJ, Krebs EG. 1974. Activation of protein kinase by physiological
255 concentrations of cyclic AMP. *Proc Natl Acad Sci U S A*. doi:10.1073/pnas.71.9.3580

256 Church TW, Tewatia P, Hannan S, Antunes J, Eriksson O, Smart TG, Kotaleski JH, Gold MG.
257 2021. Akap79 enables Calcineurin to directly suppress protein Kinase a activity. *Elife*
258 **10**. doi:10.7554/eLife.68164

259 Francis SH, Corbin JD. 1994. Structure and Function of Cyclic Nucleotide-Dependent
260 Protein Kinases. *Annu Rev Physiol*. doi:10.1146/annurev.ph.56.030194.001321

261 Gaffarogullari EC, Masterson LR, Metcalfe EE, Traaseth NJ, Balatri E, Musa MM, Mullen D,
262 Distefano MD, Veglia G. 2011. A myristoyl/phosphoserine switch controls cAMP-
263 dependent protein kinase association to membranes. *J Mol Biol*.
264 doi:10.1016/j.jmb.2011.06.034

265 Gold MG. 2019. Swimming regulations for protein kinase A catalytic subunit. *Biochem Soc*
266 *Trans*. doi:10.1042/BST20190230

267 Harvey CD, Yasuda R, Zhong H, Svoboda K. 2008a. The spread of Ras activity triggered by
268 activation of a single dendritic spine. *Science (80-)* **321**:136–140.
269 doi:10.1126/science.1159675

270 Harvey CD, Yasuda R, Zhong H, Svoboda K. 2008b. The spread of Ras activity triggered by
271 activation of a single dendritic spine. *Science (80-)* **321**:136–140.
272 doi:10.1126/science.1159675

273 Ilouz R, Lev-Ram V, Bushong EA, Stiles TL, Friedmann-Morvinski D, Douglas C, Goldberg G,
274 Ellisman MH, Taylor SS. 2017. Isoform-specific subcellular localization and function of
275 protein kinase a identified by mosaic imaging of mouse brain. *Elife* **6**.
276 doi:10.7554/eLife.17681

277 Johnson DA, Akamine P, Radzio-Andzelm E, Madhusudan, Taylor SS. 2001. Dynamics of
278 cAMP-dependent protein kinase. *Chem Rev*. doi:10.1021/cr000226k

279 Kopec CD, Li B, Wei W, Boehm J, Malinow R. 2006. Glutamate receptor exocytosis and spine
280 enlargement during chemically induced long-term potentiation. *J Neurosci* **26**:2000–
281 2009. doi:10.1523/JNEUROSCI.3918-05.2006

282 Ma L, Day-Cooney J, Benavides OJ, Muniak MA, Qin M, Ding JB, Mao T, Zhong H. 2022.
283 Locomotion activates PKA through dopamine and adenosine in striatal neurons.
284 *Nature* **611**:762–768. doi:10.1038/s41586-022-05407-4

285 Matsuzaki M, Honkura N, Ellis-Davies GCR, Kasai H. 2004. Structural basis of long-term
286 potentiation in single dendritic spines. *Nature* **429**:761–766.
287 doi:10.1038/nature02617

288 Miyamoto E, Kuo JF, Greengard P. 1969. Cyclic nucleotide-dependent protein kinases. 3.
289 Purification and properties of adenosine 3',5'-monophosphate-dependent protein

290 kinase from bovine brain. *J Biol Chem* **244**:6395–6402.

291 Otmakhov N, Lisman J. 2012. Measuring CaMKII concentration in dendritic spines. *J*
292 *Neurosci Methods*. doi:10.1016/j.jneumeth.2011.09.022

293 Pologruto TA, Sabatini BL, Svoboda K. 2003. ScanImage: Flexible software for operating
294 laser scanning microscopes. *Biomed Eng Online* **2**:13. doi:10.1186/1475-925X-2-13

295 Reimann EM, Brostrom CO, Corbin JD, King CA, Krebs EG. 1971. Separation of regulatory
296 and catalytic subunits of the cyclic 3′, 5′-adenosine monophosphate-dependent
297 protein kinase(s) of rabbit skeletal muscle. *Biochem Biophys Res Commun* **42**.
298 doi:10.1016/0006-291X(71)90086-6

299 Smith FD, Esseltine JL, Nygren PJ, Veesler D, Byrne DP, Vonderach M, Strashnov I, Eyers CE,
300 Eyers PA, Langeberg LK, Scott JD. 2017. Local protein kinase A action proceeds
301 through intact holoenzymes. *Science (80-)* **356**. doi:10.1126/science.aaj1669

302 Smith FD, Reichow SL, Esseltine JL, Shi D, Langeberg LK, Scott JD, Gonen T. 2013. Intrinsic
303 disorder within an AKAP-protein kinase A complex guides local substrate
304 phosphorylation. *Elife* **2013**. doi:10.7554/eLife.01319.001

305 Stoppini L, Buchs PA, Muller D. 1991. A simple method for organotypic cultures of nervous
306 tissue. *J Neurosci Methods*. doi:10.1016/0165-0270(91)90128-M

307 Thomas MJ, Moody TD, Makhinson M, O'Dell TJ. 1996. Activity-dependent β-adrenergic
308 modulation of low frequency stimulation induced LTP in the hippocampal CA1 region.
309 *Neuron* **17**:475–482. doi:10.1016/S0896-6273(00)80179-8

310 Tillo SE, Xiong WH, Takahashi M, Miao S, Andrade AL, Fortin DA, Yang G, Qin M, Smoody BF,
311 Stork PJS, Zhong H. 2017. Liberated PKA Catalytic Subunits Associate with the
312 Membrane via Myristoylation to Preferentially Phosphorylate Membrane Substrates.
313 *Cell Rep* **19**:617–629. doi:10.1016/j.celrep.2017.03.070

314 Vallee RB, DiBartolomeis MJ, Theurkauf WE. 1981. A protein kinase bound to the projection
315 portion of MAP 2 (microtubule-associated protein 2). *J Cell Biol* **90**.
316 doi:10.1083/jcb.90.3.568

317 Walker-Gray R, Stengel F, Gold MG. 2017. Mechanisms for restraining cAMP-dependent
318 protein kinase revealed by subunit quantitation and cross-linking approaches. *Proc*
319 *Natl Acad Sci U S A* **114**:10414–10419. doi:10.1073/pnas.1701782114

320 Weisenhaus M, Allen ML, Yang L, Lu Y, Nichols CB, Su T, Hell JW, Mcknight GS. 2010.
321 Mutations in AKAP5 disrupt dendritic signaling complexes and lead to
322 electrophysiological and behavioral phenotypes in mice. *PLoS One* **5**.
323 doi:10.1371/journal.pone.0010325

324 Wong W, Scott JD. 2004. AKAP signalling complexes: Focal points in space and time. *Nat*
325 *Rev Mol Cell Biol*. doi:10.1038/nrm1527

326 Xiong WH, Qin M, Zhong H. 2021. Myristoylation alone is sufficient for PKA catalytic
327 subunits to associate with the plasma membrane to regulate neuronal functions. *Proc*
328 *Natl Acad Sci U S A* **118**. doi:10.1073/pnas.2021658118

329 Zaccolo M, De Giorgi F, Cho CY, Feng L, Knapp T, Negulescu PA, Taylor SS, Tsien RY, Pozzan

330 T. 2000. A genetically encoded, flourescent indicator for cyclic AMP in living cells. *Nat*
331 *Cell Biol* **2**:25–29. doi:10.1038/71345

332 Zhang P, Ye F, Bastidas AC, Kornev AP, Wu J, Ginsberg MH, Taylor SS. 2015. An Isoform-
333 Specific Myristylation Switch Targets Type II PKA Holoenzymes to Membranes.
334 *Structure*. doi:10.1016/j.str.2015.07.007

335 Zhong H, Sia GM, Sato TR, Gray NW, Mao T, Khuchua Z, Huganir RL, Svoboda K. 2009.
336 Subcellular Dynamics of Type II PKA in Neurons. *Neuron* **62**:363–374.
337 doi:10.1016/j.neuron.2009.03.013

338

339 **Figures and figure legends**

340 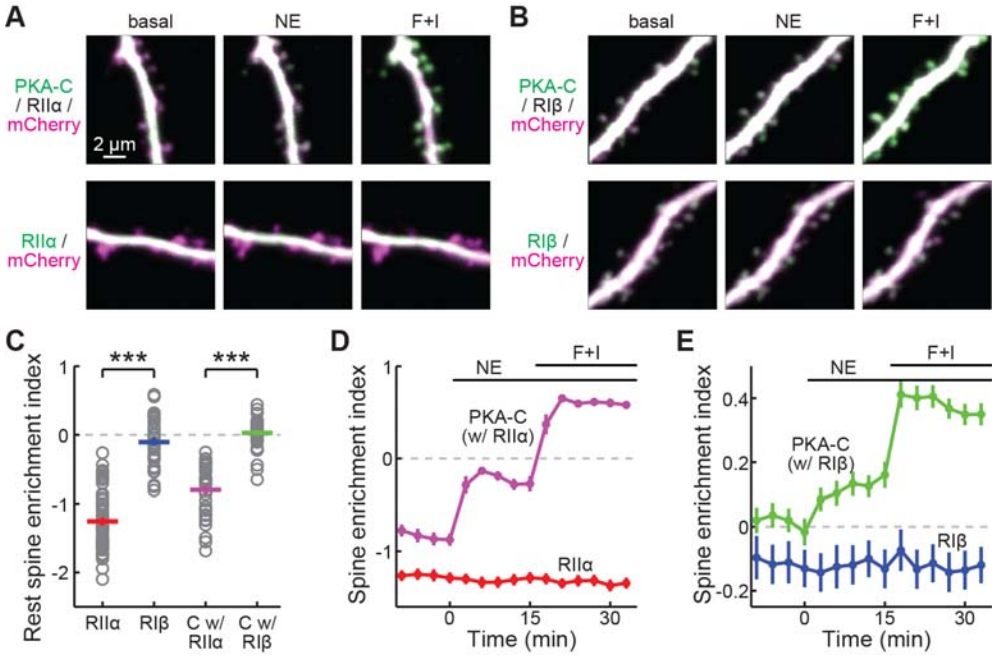

341 **Figure 1**. PKA-C but not PKA-R redistributes to spines upon activation. (A, B)
342 Representative two-photon images of PKA-C-mEGFP co-expressed with PKA-RIIα or PKA-
343 RIβ at rest, or in the presence of norepinephrine (NE) or forskolin and IBMX (F + I).
344 mCherry (magenta) was co-expressed to reveal the neuronal morphology. (C–E)
345 Quantification and comparison of the spine enrichment index at the resting state (C) and
346 upon activation (D & E). As in panel C from left to right, n (spines/neurons) = 53/11, 34/7,
347 33/6, and 36/7.

348

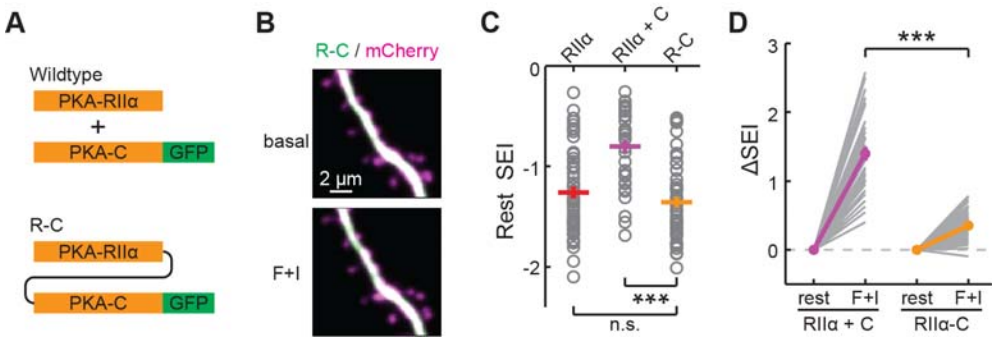

Figure 2. Characterization of the inseparable R-C. (A) Schematic of wildtype PKA versus R-C. In both cases PKA-C was C-terminally tagged by mEGFP. (B–C) Representative images (B), quantifications of resting distribution (C), and the distribution change upon stimulation by forskolin and IBMX (D) of R-C compared to PKA-RIIα-mEGFP and co-expressed PKA-C-mEGFP/PKA-RIIα. RIIα and RIIα+C data are from Fig. 1C. n (spines/neurons) = 48/10.

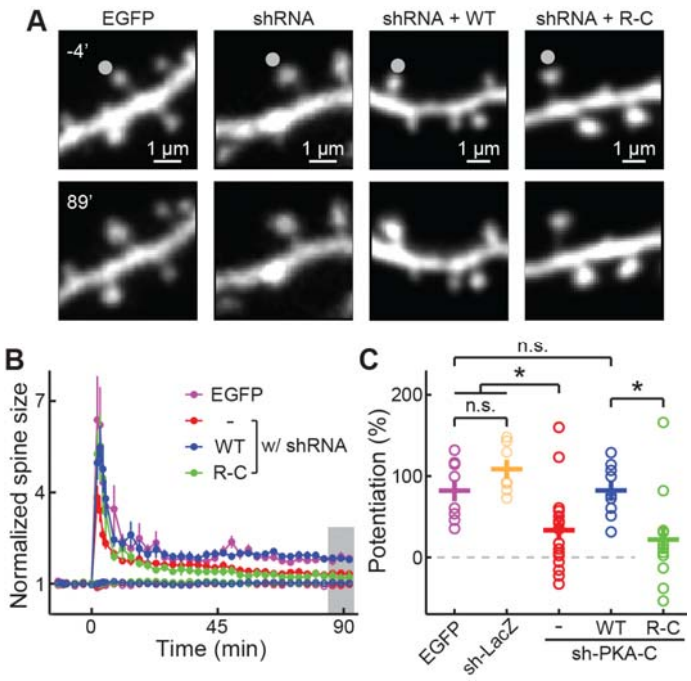

357

358 **Figure 3**. PKA regulation of synaptic plasticity cannot be sustained by an inseparable PKA

359 variant. (A–C) Representative image (A), time course (B), and the degree of potentiation (C)

360 at the indicated timepoints in panel B of single-spine LTP experiments as triggered by focal

361 glutamate uncaging at the marked spines (gray dot). In panel B, both stimulated spines

362 (solid circles) and non-stimulated control spines (open circles) are shown. As in panel C

363 from left to right, n (spines, each from a different neuron) = 8, 7, 17, 11, 9.

364

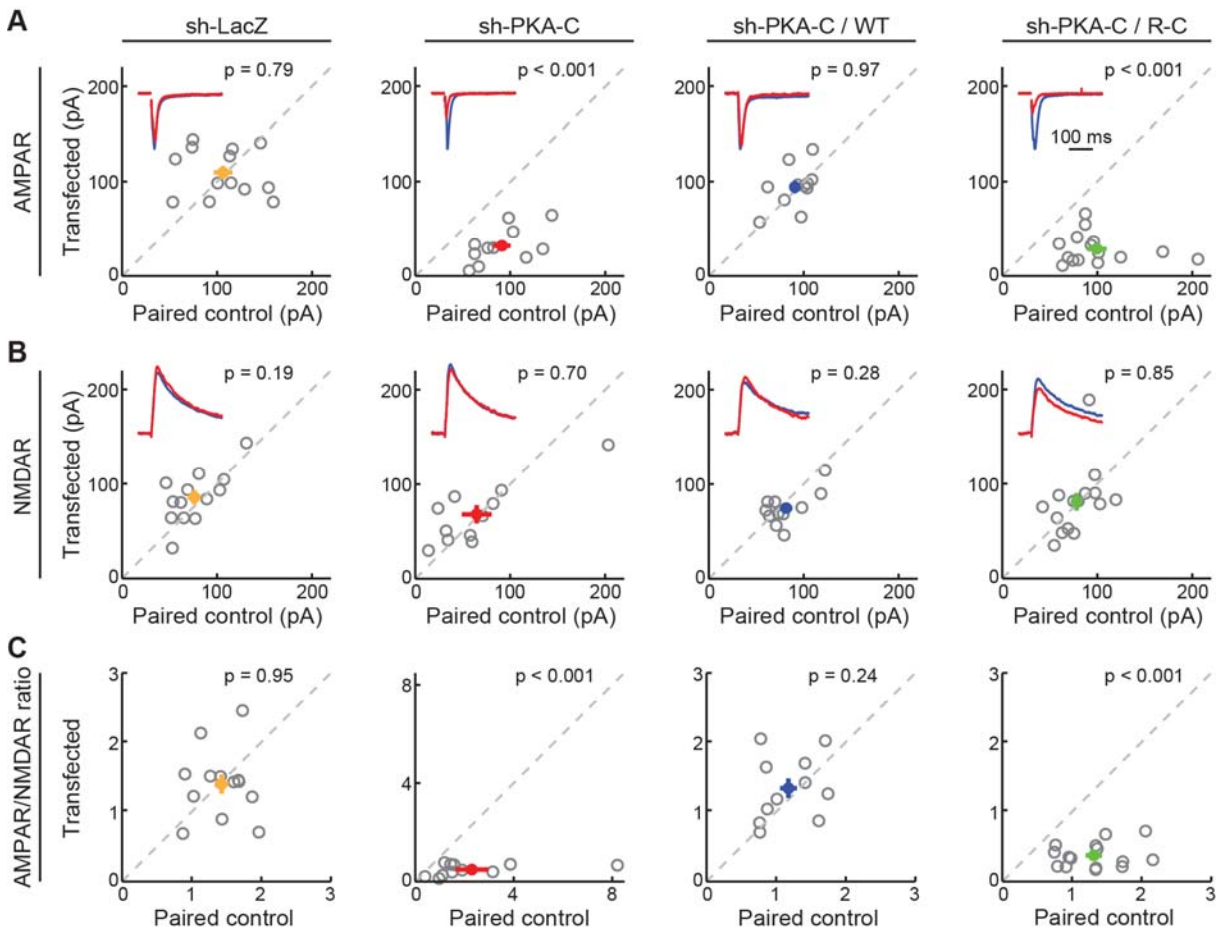

Figure 4. AMPA receptor-mediated synaptic transmission requires wildtype dissociable PKA. (A–C) Representative traces (red) normalized to the paired control (blue) (insets) and scatter plots of paired AMPA (A) and NMDA (B) receptor currents and AMPA/NMDA receptor current ratios (C) from neighboring untransfected CA1 neurons and those transfected with shRNA against PKA-C and the indicated shRNA-resistant rescue constructs. Statistical p values were obtained using a sign test (MATLAB). From left to right, n (neuron pairs) = 13, 11, 11, and 15.

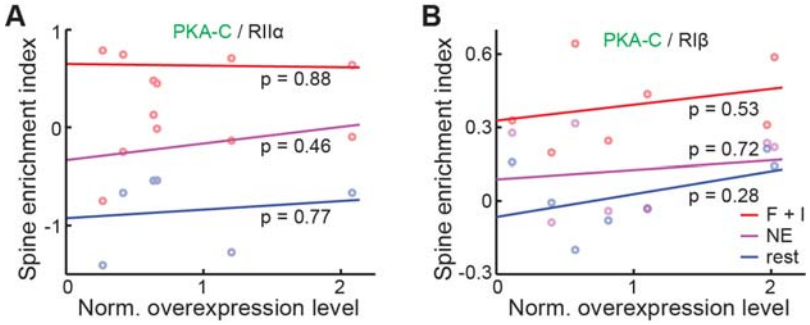

Figure 1–figure supplement 1. Spine enrichment indexes and the movement of PKA-C into spines upon activation are not dependent on the protein expression level. (A–B) Averaged spine enrichment indexes within individual neurons of PKA-C co-expressed with RIIα (A) and RIβ (B), and their linear fit at rest or under the indicated stimulation.

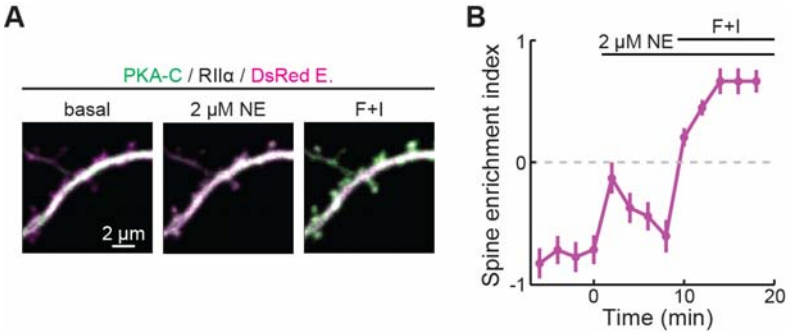

380

381 **Figure 1–figure supplement 2**. PKA-C translocation can be driven by norepinephrine at

382 low concentrations. (A, B) Representative two-photon images (A) and the collective trace of

383 PKA-C-mEGFP co-expressed with PKA-RIIα at rest, or in the presence of 2 μM

384 norepinephrine (NE) or forskolin and IBMX (F + I). DsRed Express (magenta) was co-

385 expressed to reveal the neuronal morphology. n (spines/neurons) = 16/4.

386

387

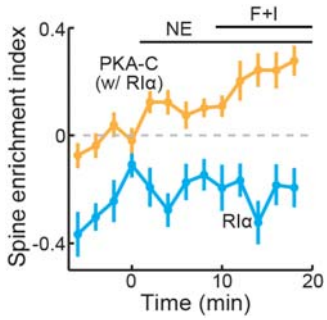

388 **Figure 1–figure supplement 3**. PKA-C and PKA-RIα differentially re-distributed upon

389 activation. The collective trace of PKA-C-mEGFP co-expressed with PKA-RIα (orange) and

390 PKA-RIα-mEGFP (light blue) at rest, or in the presence of 10 μM norepinephrine (NE) or

391 forskolin and IBMX (F + I). DsRed Express was co-expressed to reveal the neuronal

392 morphology. n (spines/neurons) = 20/5 for PKA-C and 16/4 for RIα.

393